Molecular-dynamics Study on Crack Growth Behavior Relevant to Crystal Nucleation in Amorphous Metal

R. Matsumoto[1], M. Nakagaki[1], A. Nakatani[2], H. Kitagawa[2]

Summary

The internal structural changes around the crack-tip and the pertinent crack growth behavior in an amorphous metal are studied by a large scale molecular dynamics (MD) simulation. The Finnis-Sinclair potential for α-iron is used as an interatomic potential. The model amorphous metal was created by melting-rapid quenching simulation. The crack opens in similar fashion and it has smooth surfaces during the amorphous state. As it deformed, nano-scaled crystalline phase grows around the crack-tip. The distribution of deformation zones and deformation mechanism are significantly altered. The grains are not deformed while they are relatively small. The emission of dislocations from the crack-tip is observed, after the crystal phase covered the crack-tip surfaces. The grain size appeared small in the vicinity of the crack-tip, and becomes gradually large as it separates form the crack-tip. Although CTOD obtained from MD analysis agrees to Dugdale's model very well during the amorphous state, the crack opening behavior changes remarkably after the crystallization. The peak of the stress existing ahead of the crack gradually vanishes as crystal phase grows, and the stress distribution becomes flat and the value becomes small rather than the linear elastic solution. After the crystallization, the stress increases again.

Introduction

Amorphous metal has been spotlighted as an innovative and important material in the engineering field because of its inherently high strength and a lot of unique properties. Production of only a thin film was possible at the beginning, however the recent developments of the innovative production technology had made it possible to produce bulk amorphous metal with 1∼100mm thickness [1]. It is thought that amorphous metal will be increasingly employed for industrial products.

In recent studies in the literature, it has been reported that nano-sized particles are precipitated due to plastic deformations in amorphous metal[2][3]. These results suggest that the strength of the amorphous metal is much relevant to the evolving crystal phase during fracture process. It is becoming more important to estimate with higher accuracy the mechanical properties of the material by accounting for such a microscopic internal structure change for the adequate safety. The phenomenon of the deformation induced nano-crystallization are not fully understood yet, because it is inequilibrium phenomenon which arises inside the material and the experimental observation of the atomistic structure changes in the amorphous is extremely difficult.

In this paper, the internal structural phenomena in severely deformed zones are investigated and the consequent change of fracture behavior caused by deformation induced nano-crystallization in an amorphous metal are studied. A large scale molecular-dynamics (MD) simulations of crack growth are performed in order to collect the informations due to the atomic rearrangements.

Model and Simulation Method

MD is a simulation method which can estimate various properties of materials by tracing trajectories of all particles in a system by solving Newton's equations numerically. In order to perform

[1]Department of Mechanical Systems Engineering, Faculty of Computer Science and Systems Engineering, Kyushu Institute of Technology
[2]Department of Adaptive Machine Systems, Graduate School of Engineering, Osaka University

the large scale and long time simulation, we used the domain decomposition method for the parallel caluculation using a PC-cluster. The velocity Verlet's method and the velocity scaling are applied to the time evolution and the temperature control, respectively.

The amorphous metal model used for the crack growth simulation is assumed to be made from Fe, in which the interatomic force is derived by the Finnis-Sinclair (FS) potential [4][5]. In this research, we performed the analysis modeling in the following process (see Figure 1) followed by a crack growth simulation.

1. Generation of amorphous plate

   A plate with amorphous structure was generated by a melting-rapid quenching simulation which is a similar procedure to Ref.[6]. In this research, we deal with a quasi 3-dimensional model by taking the small thickness in order to reduce the calculation and to avoid the difficulty of the data analysis. The size of the amorphous plate is 104.6 nm $\times$ 104.6 nm $\times$ 1.74 nm, containing 1,555,200 atoms. We have confirmed that the amorphous plate does not contain any clusters of crystal structures by Voronoi's polyhedron analysis.

2. Fabrication of circular model

   A disk whose radius is $R = 50$ nm is cut out from the amorphous plate. Boundary region which is fixed during the simulation is defined, as shown in Figure 1 by the shaded area within $R_{\mathrm{b}} = 0.7$ nm distance from the outer edge. The atoms in the boundary region are called as "boundary atom". The number of atoms is $N = 1,117,086$ and the number of the boundary atoms is $N_{\mathrm{b}} = 31,117$.

3. Setting of initial crack

   In order to analyze the crack growth characteristics in an infinite domain, the crack-tip is assumed to be located at the center of the disk. And then a crack is introduced into the disk by giving displacement to each atom that is obtained from the linear elastic solution of mode I stress intensity factor $K_0^{\mathrm{I}} = 0.4\ \mathrm{MPa}\sqrt{\mathrm{m}}$ under plane strain condition. In the process, the elastic properties (Young's modulus $E = 146.4$ GPa and Poisson's ratio ν=0.26) that are obtained by the simulation of uniaxial tensile deformation are used.

4. Coordinates and periodic boundary condition

   We set the origin at the crack-tip, i.e. the center of the disk. The x-direction is defined forward in the crack plane, and the z-direction in the thickness direction. The periodic boundary condition is applied to the z-direction, therefore it is deformed under near plane-strain condition ($\bar{\varepsilon_{\mathrm{z}}}$=0).

5. Initial temperature

   The initial velocities are given to all atoms according to the Maxwell's distribution equivalent to $T_0 = 600$ K. The melting point of the material is $T_{\mathrm{m}} = 2,565$ K. Therefore the relative temperature is $T_{\mathrm{r}} \equiv T_0/T_{\mathrm{m}} = 0.234$. We observed the deformation induced nano-crystallization in the case of the initial temperature is low, while it needs large deformation [7]. The purpose of this paper is show the influence of the crystallization on the crack growth behavior, thus the initial temperature is set relatively high.

6. Relaxation

   A calculation for relaxation is performed during 100 ps under 600 K. The boundary atoms are fixed during the calculation. The crack closure of $\Delta a_{\mathrm{r}} = 6.2$ nm is recognized during the relaxation. The entire structure of the domain after the relaxation is shown in Figure 2.

7. Crack growth simulation

The boundary atoms are moved with the equivalent velocity in accordance with the increasing rate of stress intensity factor $\dot{K}^{\mathrm{I}} = 2 \times 10^9$ MPa$\sqrt{\mathrm{m}}$/s. The average velocity of the boundary atoms is $v_{\mathrm{ave}} \simeq 2.998$ m/s. For the detailed data analysis, stress components, coordinates and potential energy of each atoms averaged for 1 ps are output every 10 ps. The present MD simulation was performed up to t =1,200 ps($K^{\mathrm{I}} = 2.8$ MPa$\sqrt{\mathrm{m}}$).

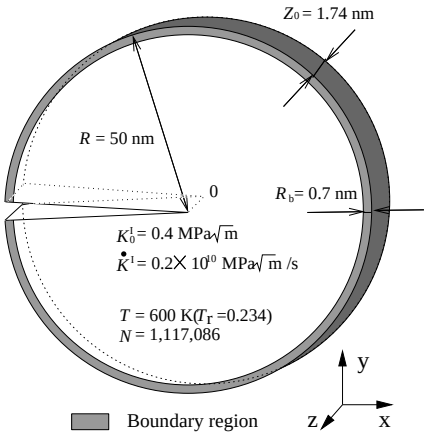

Figure 1: Simulation model

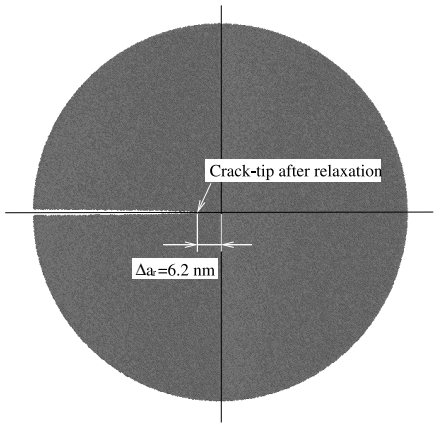

Figure 2: Initail state

Result and Discussions

Figure 3 shows the potential energy change, kinetic energy change and total energy change of the system from the initial state. Time change of the total energy is equivalent to the external work. The figure also shows the average temperature change converted from the kinetic energy. The potential energy increases gradually and starts to decrease rapidly from around $t = 700$ ps. The temperature increases with reduction in potential energy and, finally it goes up to $T = 1000$ K or more. As you can see later, this is caused by the crystallization around the crack-tip. The time differentiation of the total energy energy (i.e. external power profile) is shown in Figure 4. At the beginning, although it increases, it changes to decreasing and it increases again around $t = 1000$ ps. As shown later, crystallization progresses in the section where external work is decreasing, and crystallization is completed mostly in the section where external work is increasing again.

The shapes of the crack and the distributions of the equivalent strain increment $\Delta\bar{\varepsilon}$ are shown in Figure 5. In order to observe microscopic deformation properties, we evaluate the local values of strain with the use of a weighted means scheme. The time interval used to estimate the strain increment is 10 ps. During the amorphous state, the process zone deforms due to the generation and disappearance of the severely deformation local zones time by time. The crack opens in a similar fashion with smooth and round surfaces. Some circular regions with suppressed deformation appeared around the crack-tip at about 600 ps. As shown later, these regions have crystalline phase. The distribution of the deformation zones are significantly altered, as they grow. The grains are not deformed while they remain relatively small. Most amorphous-crystal interfaces have large strain increment for

phase transition. The emanated dislocations from the crack-tip are observed after the crystal phase covers the crack-tip surfaces. First, crystals nucleate from points off the crack-tip followed by subsequent nucleation on the crack surfaces. This result suggests the crystallization behavior is influenced not only temperature but also stress and strain rate. The grain size is small near the crack-tip, and it appears gradually large as it separates from the crack-tip. The smallest grain is smaller than 10 nm.

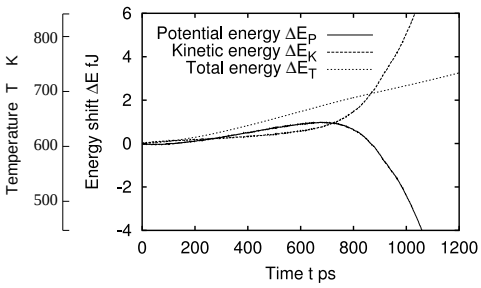

Figure 3: Energy profile

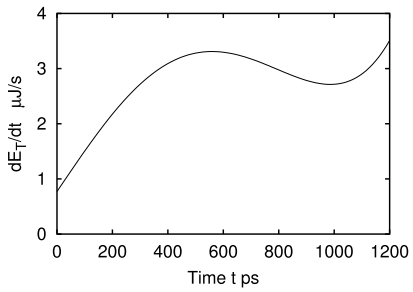

Figure 4: Derivative of E_{T}

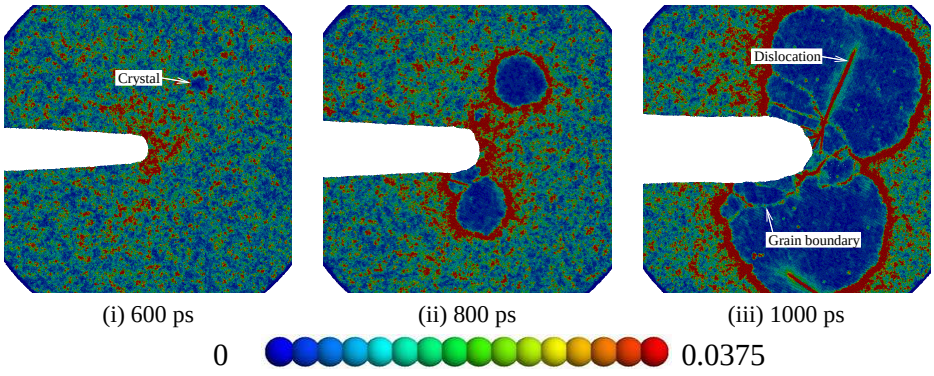

Figure 5: Distribution of the equivalent strain increment $\Delta\bar{\varepsilon}$

Figure 6 shows the change of the crack extension Δa and the crack-tip opening displacement (CTOD) b. The amount of crack extension was evaluated on the basis of the crack-tip position after the relaxation calculation (Figure 2). The stress intensity factor K^{I} of each time is also shown in the horizontal axis. Furthermore, the least mean square approximation of the amount of crack extension from 0 ps to 800 ps is also shown. We used the 3rd function for the approximation. Roughly speaking amorphous metal behaves like a perfect plastic material, the figure also gives CTOD b_D obtained from Dugdale's model in plane strain. The CTOD b_D was calculated using the following formulas.

$$b_{\mathrm{D}} = \frac{K^{\mathrm{I}2}}{E'\sigma_{\mathrm{Y}}} = \frac{(K_0^{\mathrm{I}} + \dot{K}^{\mathrm{I}}t)^2(1-\nu^2)}{E\sigma_{\mathrm{Y}}} \tag{1}$$

Here, σ_Y is the yield stress and we used $\sigma_Y = 1.8$ GPa which is evaluated from the equivalent stress at the crack-tip averaged from $t = 400$ ps to $t = 600$ ps. In the amorphous state, it turns out that CTOD obtained from MD analysis b agrees to Dugdale's model b_D very well during the amorphous state. Similar results have been obtained experimentally [8]. The amount of the crack extension Δa increases monotonously. However, as you can recognize, the amount of increase of the crack extension becomes large during $t = 800 \sim 900$ ps. We suppose that it was caused by the deformation accompanying the crystallization. After $t = 900$ ps, since the crack front region changes to polycrystalline structures, material hardens and, the amount of the crack extension Δa and CTOD increase become small.

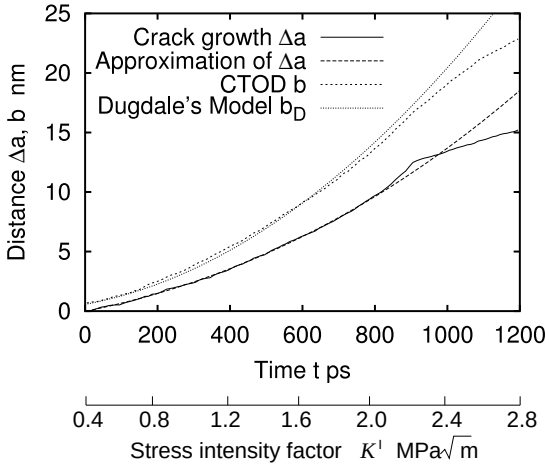

Figure 6: Crack extension Δa and CTOD b

The distribution of the stress of the perpendicular direction in the crack plane (σ_θ) is shown in Figure 7. Along the horizontal axis, the distance from the crack-tip r at each time is taken, and the distance normalized by CTOD r/b is also shown simultaneously. The chained line in each figure shows the linear elastic solution obtained from the stress intensity factor K^{I} at each time. During the amorphous state, we can find that the linear elastic solution agrees to the result of the MD analysis very well in the region $r/b > 2$. The peak of the stress which exist around $r/b \simeq 1$ until $t = 600$ ps gradually vanishes as crystal phase grows, and the stress distribution becomes flat and the value becomes small rather than the linear elastic solution (see. Figure (c)). The stress increases again when crystallization around the crack-tip finishes mostly (see. Figure (d)). These results suggest a possibility of large deformation during crystallization by low stress.

Conclusions

We performed a large scale MD simulation of crack growth in an amorphous metal in order to investigate the internal structure change around the crack-tip and crack extension behavior.

- Amorphous metal is nano-crystallized by severe deformation. Some clusters nucleate around the crack-tip and they grow rapidly. The grain size is small near the crack-tip, and it appears gradually large as it separates from the crack-tip.

- The distribution of deformation zones and deformation mechanism are significantly altered, as crystalline phase grow. The emission of dislocations from the crack-tip is observed after the crystal phase covers the crack-tip surfaces.
- The stress in the crack front decreases temporarily by the deformation accompanying the crystallization.

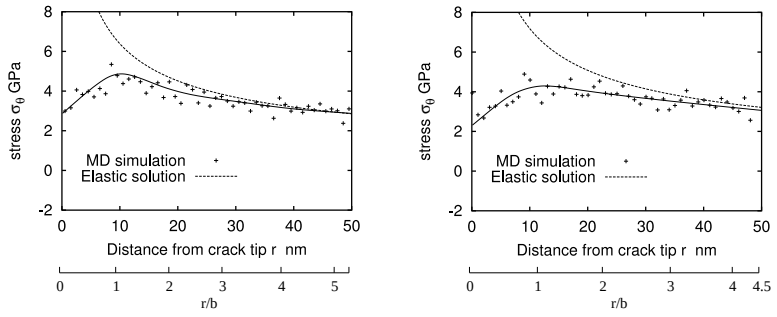

(i) 600 ps (ii) 700 ps

(iii) 800 ps (iv) 1000 ps

Figure 7: Stress distribution in front of the crack-tip

Reference

1. A. Inoue, (2000), *Acta. Mater*, **48**, 279-306.
2. T.G. Nieh, J. Wadsworth, C.T. Liu, T. Ohkubo and Y. Hirotsu, (2001), *Acta. Mater*, **49**-15, 2887-2896.
3. J.C. Lee, Y.C. Kim, J.P. Ahn, H.S. Kim, S.H. Lee and B.J. Lee, (2004), *Acta. Mater*, **52**-15, 1525-1533.
4. Finnis, M. W. and Sinclair, J. E., (1984), *Philos. Mag.*, A, **50**-653, 45-55.
5. Finnis, M. W. and Sinclair, J. E., (1986), *Philos. Mag.*, A, **53**-1, 161.
6. Nakatani, K., Nakatani, A., Sugiyama, Y. and Kitagawa, H., (2000), *AIAA Journal*, **38**-4, 695-701.
7. Matsumoto, R., Kitagawa, H. and Nakatani, A., (2003), *Journal of The Society of Materials Science Japan*, Vol. 52-3, pp.235-240(in japanese).
8. Flores, K. M. and Dauskardt, R. H., (1999), *Scripta metall.*, **41**-9, 937-943.